Organic & Biomolecular Chemistry

PAPER

View Article Online
View Journal | View Issue

Cite this: *Org. Biomol. Chem.*, 2016, **14**, 1715

Structure of olefin–imidacloprid and gas-phase fragmentation chemistry of its protonated form†

Roberto Fusetto, Jonathan M. White, Craig A. Hutton and Richard A. J. O'Hair*

One of the major insect metabolites of the widely used neonicotinoid insecticide imidacloprid, **1** (1-[(6-chloro-3-pyridinyl)methyl]-*N*-nitro-1*H*-imidazol-2-amine), is the olefin **2**. To better understand how the structure of olefin **2** relates to the gas-phase fragmentation of its protonated form, $\mathbf{2H^+}$, X-ray crystallography, tandem mass spectrometry experiments and DFT calculations were carried out. Olefin **2** was found to be in a tautomeric form where the proton is on the N(1) position of the imidazole ring and forms a hydrogen bond to one of the oxygen atoms of the coplanar nitroamine group. Under conditions of low-energy collision-induced dissociation (CID) in a linear ion trap, $\mathbf{2H^+}$, formed *via* electrospray ionization (ESI), fragments *via* a major loss of water, together with minor competing losses of HNO_2 and $NO_2^{\bullet}$. This contrasts with $\mathbf{1H^+}$, which mainly undergoes bond homolysis *via* $NO_2^{\bullet}$ loss. Thus, installation of the double bond in **2** plays a key role in facilitating the loss of water. DFT calculations, carried out using the B3LYP/6-311G++(d,p) level of theory, revealed that loss of water was energetically more favourable compared to HNO_2 and $NO_2^{\bullet}$ loss. Three multistep, energetically accessible mechanisms were identified for loss of water from $\mathbf{2H^+}$, and these have the following barriers: (i) direct proton transfer from N(5) of the pyridine to O(1) on the NO_2 group (119 kJ mol^{-1}); (ii) rotation of the N(2)–N(4) bond (117 kJ mol^{-1}); (iii) 1,3-intramolecular proton transfer between the two oxygen atoms of the NO_2 group (145 kJ mol^{-1}). Given that the lowest barrier for the losses of HNO_2 and $NO_2^{\bullet}$ is 156 kJ mol^{-1}, it is likely that all three water loss mechanisms occur concurrently.

Received 18th November 2015,
Accepted 16th December 2015

DOI: 10.1039/c5ob02371h

www.rsc.org/obc

Introduction

The neonicotinoid insecticide imidacloprid, **1**, is one of the most widely used insecticides worldwide.[1] Its selective toxicity towards insects is a consequence of it binding more strongly to insect nicotinic acetylcholine receptors (nAChRs) than to their mammalian counterparts.[2,3] Its use has generated considerable recent public attention[4] due to a possible contribution to honey bee colony collapse disorder,[5] ultimately leading to its ban in the EU.[6] A range of studies has been carried out to better understand the biological consequences of exposure of insects to imidacloprid.[7–9] For example, HPLC-MS based methods have been used to study the formation of its metabolites, including the olefin metabolite **2** and the hydroxyl metabolite **3** (Scheme 1) *in vivo* for: honeybees;[10] termites;[11] houseflies[12] and the vinegar fly, *Drosophila melanogaster*.[13] X-ray and molecular modelling docking studies, carried out on the binding of imidacloprid to nAChRs, have uncovered the molecular basis for the differences in binding sites in insect *versus* vertebrate nAChRs.[14,15] Different docking studies on homology models for *Apis mellifera*[16] and *Lymnaea stagnalis* acetylcholine binding protein (AChBP)[17] and the *in vivo* electrophysiological studies on recombinant *Drosophila* SAD/chicken β2 hybrid nAChRs[18] have highlighted the different binding properties and activity of these receptor subunits towards imidacloprid. In contrast, there has only been a single report on docking studies of **2** with different α/α and α/β subunits of nAChRs of *Apis mellifera*.[16] An intriguing study on the neuroblocking potency of imidacloprid metabolites suggested that **2** and **3** (Scheme 1) are about ten times less potent than imidacloprid.[19] The molecular basis for this effect is not understood, and while an X-ray structure for **3** has been reported,[20] the X-ray structure of **2** has not been reported until now.

As part of a program aimed at examining the *in vivo* metabolism of **1** in *Drosophila melanogaster*,[13] we required a sample of **2** to examine its potency in biological tests and as both an internal standard and an authentic standard for MS studies. The synthetic method of Novák *et al.*,[21] was used to prepare

School of Chemistry, Bio21 Institute of Molecular Science and Biotechnology, and ARC Centre of Excellence for Free Radical Chemistry and Biotechnology, University of Melbourne, Melbourne, Victoria 3010, Australia. E-mail: rohair@unimelb.edu.au

†Electronic supplementary information (ESI) available: Details of the synthesis of olefin **2** and ^{1}H-NMR and mass spectra information for each synthetic product, crystallographic analysis, HRMS measurements for key fragment ions, scatter plots for the two resonance forms, QTof CID mass spectra, alternative DFT calculated mechanisms for loss of water and HNO_2. CCDC 1422950. For ESI and crystallographic data in CIF or other electronic format see DOI: 10.1039/c5ob02371h

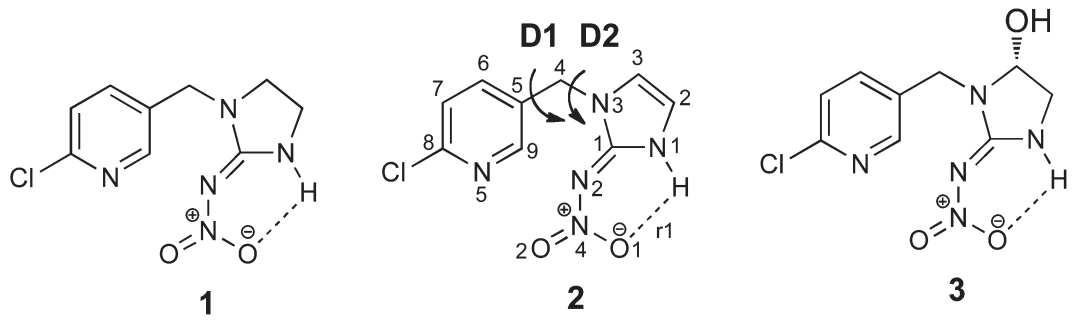

Scheme 1 Imidacloprid, **1**, and its metabolites: olefin–imidacloprid **2** and hydroxyl derivative **3**. D1 and D2 represent the key bond rotations that describe conformations of **2**.

olefin **2** to examine its structure *via* X-ray crystallography. Since tandem mass spectrometry (MS/MS) typically involves low energy collision-induced dissociation (CID) of protonated analytes and the full CID spectrum of $\mathbf{2H}^+$ has not yet been reported, we studied the fragmentation mechanism of $\mathbf{2H}^+$ in the gas phase and compared its gas-phase ion chemistry to the parent insecticide $\mathbf{1H}^+$ discussed previously.[22]

Results

X-ray crystallography

Compound **2** was recrystallised from ether and suitable crystals for X-ray diffraction were collected. The X-ray structure of olefin–imidacloprid is reported in Fig. 1, while its key structural parameters are reported in Table S1.† The thermal ellipsoid plot for compound **2** highlights that the nitroamine group is coplanar with the imidazole ring.

The formation of the N(1)–H···O(1) hydrogen bond in addition to extensive delocalization of electron density over the entire nitroamino imidazole moiety, constrains the nitroguanidinic moiety in this configuration. The N(1)–C(1)–N(2) bond angle is opened out to 133.7(3)° while the N(3)–C(1)–N(2) is closed to 119.1(2)° compared to the *ca.* 126° external bond angles expected for a substituted sp^2 hybridized atom in this 5-membered ring. The crystal packing is characterised by a bifurcated intermolecular hydrogen bond between the imidazole N(1)–H donor and the nitro oxygen O(2) and the exocyclic guanidine nitrogen N(2) (ESI, Fig. S1†).

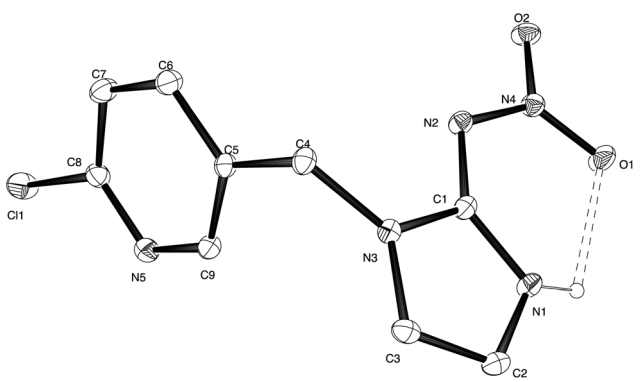

Fig. 1 Thermal ellipsoid plot for X-ray structure of olefin–imidacloprid **2**. Ellipsoids are at the 20% probability level.

As shown in Scheme 2, the nitroguanidine group in compounds such as **2** can potentially adopt two tautomeric forms. A search of the Cambridge database[23] for structures containing the nitroguanidine group located 151 structures of which 132 were represented by tautomer **A**. The remaining structures were either protonated salts or had the guanidine moiety embedded in a substituted 1,3,5-triazine derivative and were not representative of the fragment **B**.

Tautomer **A** in turn has two main resonance forms (**A1** and **A2**) generated by the delocalisation of the guanidinyl nitrogen lone pairs onto the oxygen atoms of the nitro group through the imine functional group (Scheme 2). The C–N and N–N bond distances provided information on which of these resonance forms predominates in a given structure. A scatter plot of N–N *versus* C–N bond distances from the 132 structures obtained from the Cambridge Structural Database revealed the presence of structures with differing contributions of resonance forms **A1** and **A2** (Fig. S2, ESI†). Selected structural parameters for olefin–imidacloprid, **2**, and its saturated analogue imidacloprid, **1**,[24] were compared with the average distances obtained from the 132 structures collected (Scheme 2, table). The shorter N–N bond and the longer C–N bond of **2**, suggested a significantly greater contribution to the **A2** resonance form in compound **2** compared to that of **1**.[23]

Gas-phase fragmentation of $\mathbf{2H}^+$

There have been numerous LC-MS studies in which the concentration of **1** in complex biological matrices is determined *via* MS/MS experiments where selected ion fragments are monitored upon CID of $\mathbf{1H}^+$ (the so called multiple reaction monitoring (MRM) technique).[25–27] Fewer studies have used MRM to quantify the concentrations of imidacloprid metabolites. Two recent reports have used different fragment ions of $\mathbf{2H}^+$ to quantify the concentrations of **2** in bee's wax[28] and

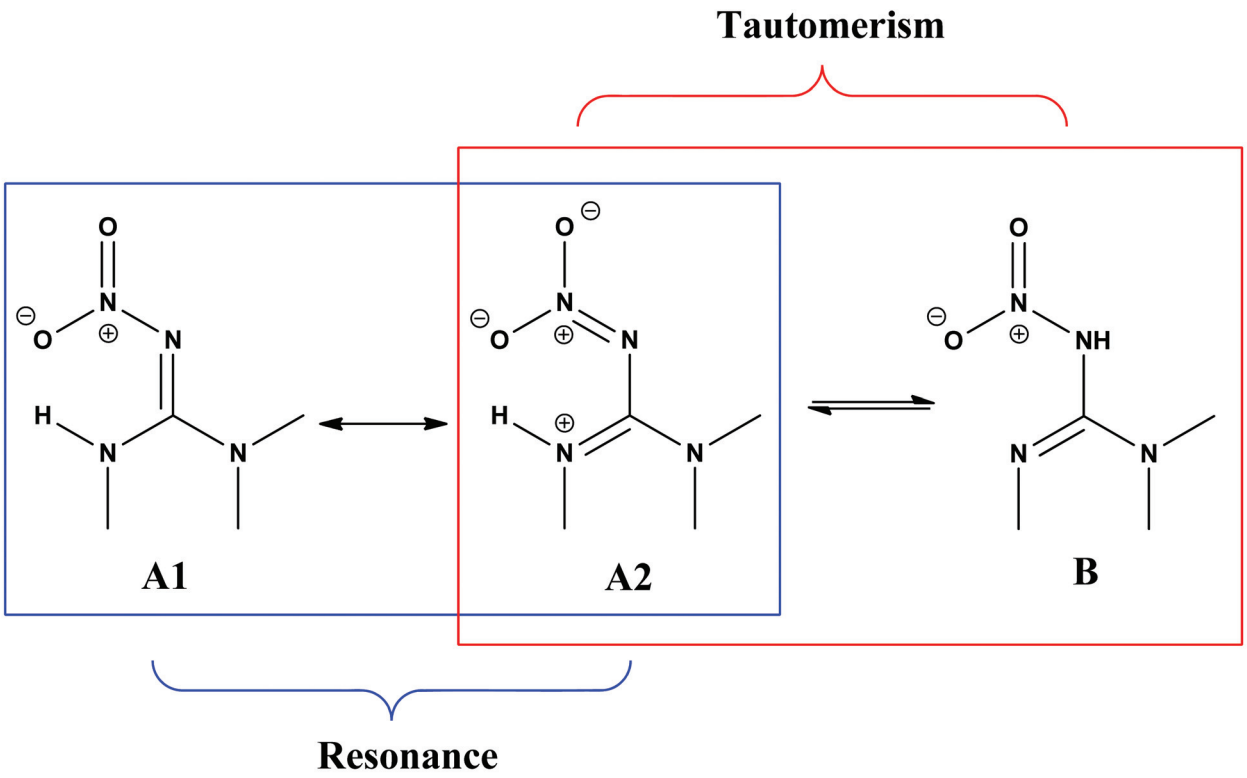

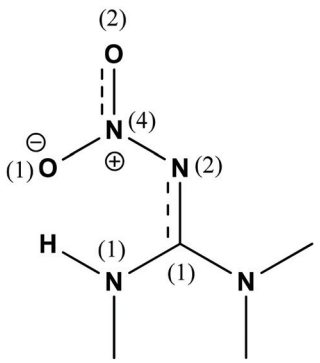

Bonds	Compound 2	Compound 1	CSD 132 Hits
N(4)-O(1)	1.246(3)	1.218(3)	1.246
N(4)-O(2)	1.249(3)	1.220(3)	
N(2)-N(4)	1.327(3)	1.337(3)	1.332
C(1)-N(2)	1.355(3)	1.336(3)	1.360

Scheme 2 The two possible tautomeric forms of **2** and the resonance forms deriving from the tautomer **A**. A comparison among the selected structural parameters (values in Å) obtained from the Cambridge Structural Database using the search fragment **A** (table below) with olefin–imidacloprid (compound **2**) and imidacloprid (compound **1**)[24] suggest that **2** is best represented by the resonance form **A2**, whereas resonance form **A1** is more likely to represent **1**.

honeybee and honey samples.[29] In the former study, the transitions *m/z* 254 → *m/z* 205 and *m/z* 254 → *m/z* 171 were used, while the later utilized *m/z* 254 → *m/z* 236 and *m/z* 254 → *m/z* 171. Given that the full CID spectrum of $\mathbf{2H}^+$ does not appear to have been reported, we examined its fragmentation reactions under low energy CID conditions in ion trap and QTof mass spectrometers. Mass selection of $\mathbf{2H}^+$ (*m/z* 254), formed in high abundance upon electrospray ionization of **2**, followed by CID in the linear ion trap mass spectrometer, gave three main fragment ions (Fig. 2): *m/z* 236 corresponding to water loss (eqn (1)); *m/z* 208 corresponding to $NO_2^{\bullet}$ loss (eqn (2)) and *m/z* 207 corresponding to HNO_2 loss (eqn (3)) (Fig. 2). These assignments were confirmed by High Resolution Mass Spectrometry (HRMS) on the fragment ions (ESI Table S2†). By varying the activation voltage, energy resolved CID experiments were carried out in a 3D ion trap to establish the relative onsets for these fragmentation channels. The onset for loss of water is less than that for $NO_2^{\bullet}$ and HNO_2 loss (Fig. 2B),

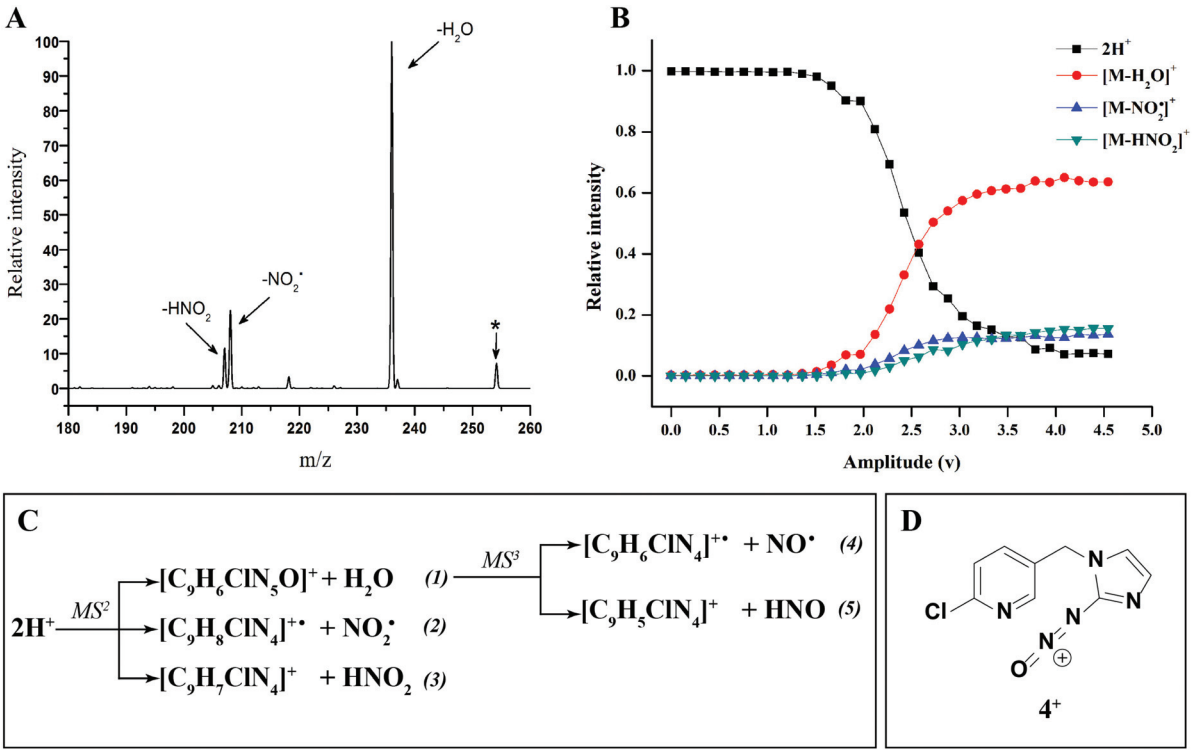

Fig. 2 (A) CID mass spectrum of $2H^+$ (*m/z* 254), obtained using the linear ion trap with normalized collision energy of 18% for 30 ms and a 1.0 *m/z* wide isolation window. The ^{35}Cl isotope was mass selected and the precursor ion is indicated by an asterisk. (B) Energy Resolved CID diagram of $2H^+$. The relative intensity of produced water shows how this pathway is highly competitive against $NO_2^{\bullet}$ and HNO_2 loss. (C) Equations reporting the MS^2 and MS^3 fragmentation products of compound $2H^+$. (D) The structure of the main product ion 4^+.

suggesting it is energetically favoured. The loss of water must involve one of the oxygen atoms of the nitro group as well as both the ionizing proton and another proton derived from **2**. In order to establish which protons are involved in this loss, H/D exchange was performed on **2** and the resultant solution was subjected to ESI/MS, giving rise to a mixture of $[M + H]^+$, $[M + D]^+$ and $[M - H + 2D]^+$ of compound **2**. The presence of ^{35}Cl and ^{37}Cl isotopes give rise to a cluster of ions from *m/z* 254 to *m/z* 258. CID of the selected $[M - H + 2D]^+$ ion at *m/z* 256 gave rise to D_2O loss (data not shown), highlighting that the N(1) proton of **2** is involved in water loss. Thus the likely structure of the ion arising from water loss is the hetero (aryl-)-*N*-nitroso-onium ion 4^+ (Fig. 2D).[30–32] The related loss of water from a nitro group that involves both the ionizing proton and a heterocyclic NH has been recently described for protonated 2-nitroimidazole.[33] As the fragment ions at *m/z* 205 and *m/z* 171 have been used in MRM transition studies of $2H^+$,[28,29] we used the multistage mass spectrometry capabilities of the linear ion trap mass spectrometer to isolate and study the fragmentation reactions of the product ion 4^+ (*m/z* 236). The major fragments in the MS^3 spectrum (ESI Fig. S3†) are ions at: *m/z* 206, which corresponds to $NO^{\bullet}$ loss (eqn (4)); and *m/z* 205, which corresponds to HNO loss (eqn (5)). The low intensity fragment ion at *m/z* 171 likely arises from the loss of the chlorine atom from the *m/z* 206 product, a reaction that occurs when the ion at *m/z* 206 is mass selected and subjected to a further stage of CID in a MS^4 experiment (data not shown). We also examined the CID spectra of $2H^+$ as a function of collision energy in a QTof mass spectrometer (ESI Fig. S4†), which confirmed that *m/z* 205 and *m/z* 171 can be formed under the multi collision conditions at higher CID energies.

Density functional calculations on the fragmentation of $2H^+$

To better understand the role of the proton in the fragmentation reactions of $2H^+$, density functional theory calculations were carried out on a range of conformers for different structural isomers in which the proton is located at different basic sites of **2** and various potential mechanisms for the competing losses of H_2O, $NO_2^{\bullet}$ and HNO_2 were investigated. The B3LYP/6-311G++(d,p) level of theory was chosen to allow direct comparison to the calculated fragmentation chemistry of $1H^+$.[22]

Sites of protonation of 2. We started our analysis on isomers of $2H^+$ by using molecular dynamic (MD) simulations to determine the lowest energy structure that best represent compound **2** in the gas-phase. The coordinates of the crystal structure of olefin–imidacloprid were analysed using the Discovery Studio (DS) 2.5 program package as described in a previous paper.[34] 100 different conformers were obtained and the 10 most stable candidate structures were selected and re-optimized using DFT calculations implemented in the

Gaussian 09 suite of programs to find the lowest energy state. The most favourable conformer resembled the crystal structure of compound **2** with the nitrogen N(5) of the pyridine group facing the opposite direction of the nitroguanidinyl group (this difference can be reasonably accommodated by favourable packing forces in the crystal structure of **2**, Fig. 1). Next, we examined the relative gas-phase stabilities of the two possible tautomeric forms of compound **2** (Scheme 2). Tautomer **A** was lower in energy than tautomer **B** by 26 kJ mol^{-1}. While tautomer **A** maintains the nitroguanidine chain locked in the conformation coplanar with the imidazole ring, as found in the crystal structure (Fig. 1), tautomer **B** showed more flexibility, with possible rotations of 90° around the C(1)–N(2) bond. We then considered the relative local proton affinities for protonation at the various possible heteroatom (N or O) sites for the most stable conformation of **2**. Protonation at the oxygen O(2) was more favourable than on the nitrogen N(5) by a few kJ mol^{-1} ($\Delta E \approx 4$ kJ mol^{-1}). Since all ten optimized structures obtained from the molecular dynamic simulations presented the same conformation of tautomer **A** but different conformations for the chloro-pyridine group, we tested if the PA on N(5) can change depending on its spatial orientation. A scan of the dihedral angle D1 (Scheme 1) was carried out and the PAs for the different heteroatoms recalculated. When the nitrogen N(5) of the chloro-pyridine was oriented toward the oxygen O(2) of the nitroguanidinyl group it became the thermodynamically favoured site of protonation in the gas-phase ($\mathbf{2H_a}^+$). A related conformation was also favoured in **1**.[22] All the DFT calculated energies reported for isomeric structures and all species (intermediates, transition states and products) associated with the fragmentation reactions are relative to this structure (see Fig. 3 for the optimized structures). The next most favourable sites for protonation and their energies relative to $\mathbf{2H_a}^+$ are: O(2) atom of the nitro group ($\mathbf{2H_b}^+$, +9 kJ mol^{-1}); N(2) atom of the nitroguanidine group ($\mathbf{2H_c}^+$, +20 kJ mol^{-1}); O(1) atom of the nitro group ($\mathbf{2H_d}^+$, +27 kJ mol^{-1}); and N(1) in the imidazolyl ring ($\mathbf{2H_e}^+$, +193 kJ mol^{-1}). Attempts to optimize a structure where protonation had occurred at N(3) were unsuccessful as the input structure dissociated *via* cleavage of the N(3)–C(4) bond to form a complex between (6-chloropyridin-3-yl) methylium ion and 2-nitro-diazine-imidazole.

Possible mechanisms for the loss of H_2O from $2H^+$. Given that the experiments show the involvement of both the ionizing proton and the N(1)–H, we focused our DFT calculations on mechanisms in which the ionizing proton and N(1)–H are transferred intramolecularly to an oxygen atom of the nitro group. The lowest energy mechanisms are shown in Fig. 4 (all activation barriers and energies of intermediates are relative to $\mathbf{2H_a}^+$ at 0 kJ mol^{-1}). There are three pathways for the intramolecular transfer of the ionizing proton from $\mathbf{2H_a}^+$ to $\mathbf{2H_d}^+$, which is the key intermediate for subsequent water loss.

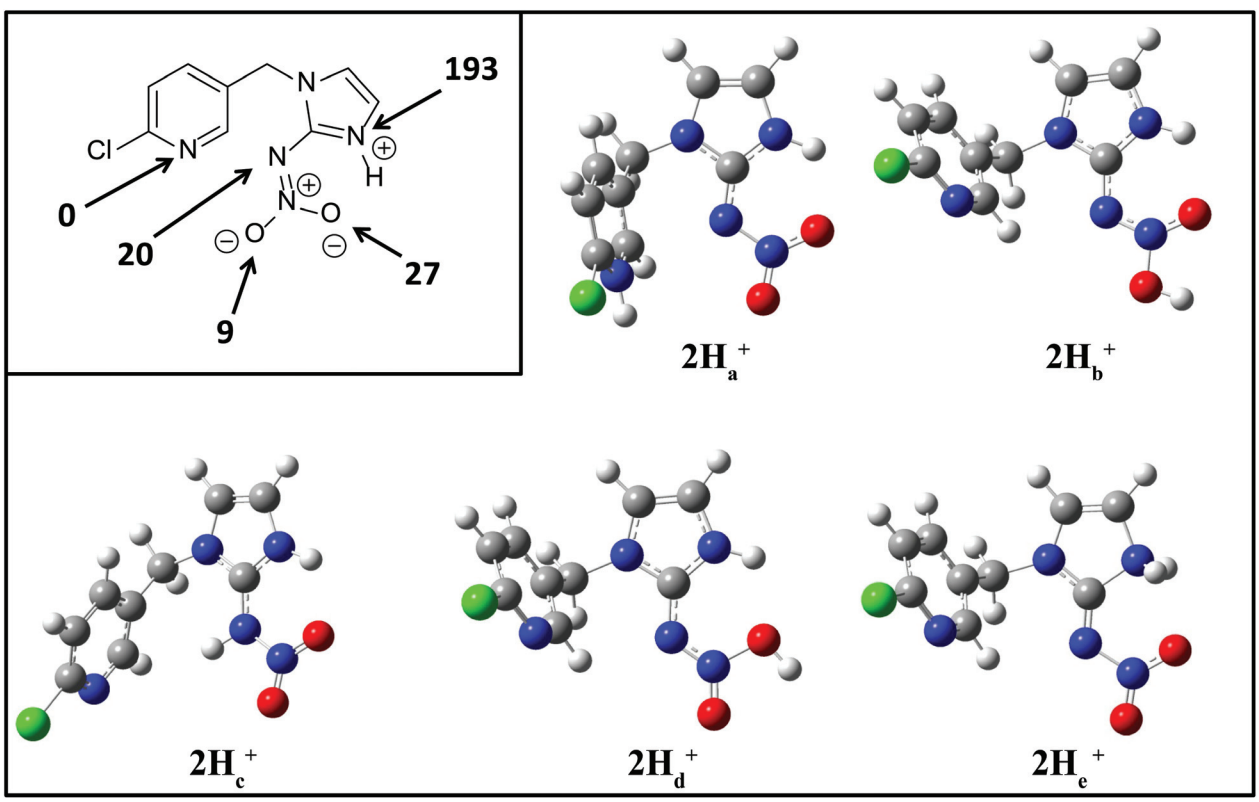

Fig. 3 B3LYP/6-311G++(d,p) DFT calculations on the gas-phase protonation of **2**. Inset shows relative local proton affinities in kJ mol^{-1}. Optimized structures are for protonation at: N(5), O(2), N(2), O(1) and N(1) designated as $\mathbf{2H_a}^+$, $\mathbf{2H_b}^+$, $\mathbf{2H_c}^+$, $\mathbf{2H_d}^+$ and $\mathbf{2H_e}^+$ respectively.

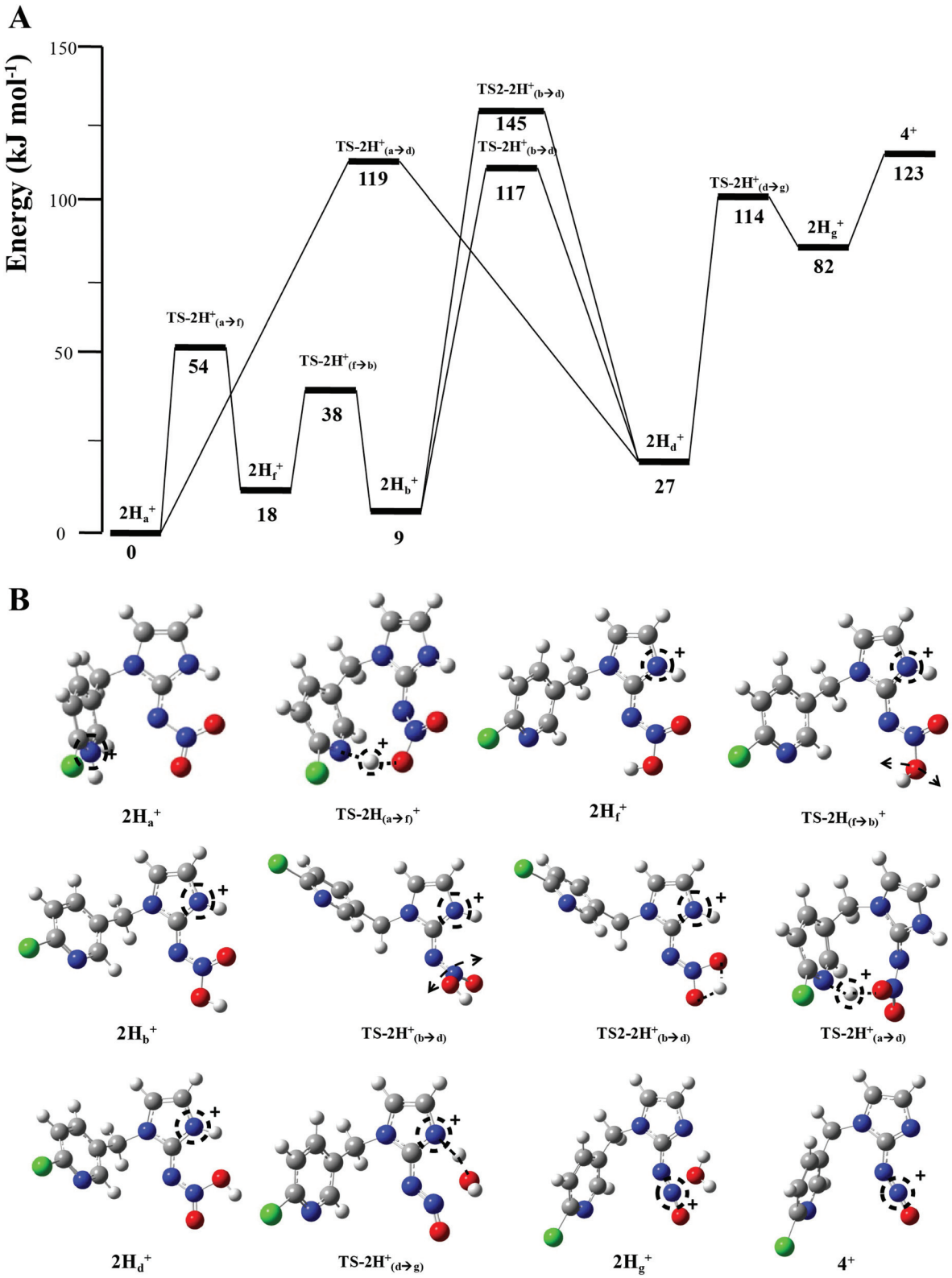

Fig. 4 B3LYP/6-311++G(d,p) DFT calculated mechanisms for H_2O loss from $2H^+$: (A) Potential energy diagram. (B) Structures of key species.

Pathway 1 involves direct proton transfer in a single step proceeding *via* **TS-2H$_{(a\rightarrow d)}^+$**, a process with an activation barrier of 119 kJ mol^{-1}. Alternatively, isomerisation can occur *via* three steps. The first step involves transfer of the ionizing proton from $2H_a^+$ to $2H_f^+$, proceeding *via* **TS-2H$_{(a\rightarrow f)}^+$** with an activation barrier of 54 kJ mol^{-1}. Subsequently, an axial inversion

of the proton on O(2) is reached through a lower activation barrier of 38 kJ mol^{-1} (**TS-2H$_{(f\rightarrow b)}$**$^+$). Pathway 2 then proceeds *via* **TS-2H$_{(b\rightarrow d)}$**$^+$ with an activation barrier of 117 kJ mol^{-1}. This process for isomerizing **2H$_b$**$^+$ to **2H$_d$**$^+$ involves an N–N bond rotation. The inverted orientation of the hydrogen in the optimised state **2H$_b$**$^+$ allows the 1,3-intramolecular proton transfer between the two oxygen atoms (pathway 3) *via* the higher energy transition state **TS2-2H$_{(b\rightarrow d)}$**$^+$ (145 kJ mol^{-1}). Once **2H$_d$**$^+$ is formed, 1,5-intramolecular proton transfer of the N(1) proton is coupled with dissociation of the N(4)–O(1) bond in **TS-2H$_{(d\rightarrow g)}$**$^+$ to yield the ion–molecule complex **2H$_g$**$^+$, with an activation barrier of 114 kJ mol^{-1}. Related intramolecular proton transfer coupled with dissociation has been described for the fragmentation of protonated glycine.[35] The alternative class of mechanism for water loss involves intramolecular H-transfer from N(1) to O(1) followed by proton transfer of the ionizing proton from N(5) (Fig. S5†), which involves a series of higher activation energies (ranging from 167 to 186 kJ mol^{-1}) and is less likely to operate under the low energy CID conditions used in the ion trap mass spectrometers.

Possible mechanisms for the losses of $NO_2^{\bullet}$ and HNO_2. The energy resolved CID reported in Fig. 2 and the DFT calculated potential energy diagram (Fig. 4) showed that the loss of water must involve lower energetic barriers compared to the loss of neutral HNO_2 and the radical $NO_2^{\bullet}$ when fragmentation of **2H$_a$**$^+$ is induced in the gas-phase. Thus we used DFT calculations to examine the energetics associated with potential mechanisms for the losses of HNO_2 and $NO_2^{\bullet}$. The lowest energy mechanisms found are shown in Fig. 5 (all activation barriers and energies of intermediates are relative to **2H$_a$**$^+$ at 0 kJ mol^{-1}). Two pathways are possible to reach the optimised state **2H$_c$**$^+$, the key intermediate in this mechanism. Pathway 1 involves the direct transfer of the proton from N(5) on the pyridine to N(2) on the nitroguanidine group through a single step transition state of 166 kJ mol^{-1} (**TS-2H$_{(a\rightarrow c)}$**$^+$). Alternatively, in pathway 2, the proton is transferred to the oxygen O(2) as described in water loss mechanism (**TS-2H$_{(a\rightarrow f)}$**$^+$, 54 kJ mol^{-1}, Fig. 4) and is subsequently transferred to N(2) with an activation barrier of 156 kJ mol^{-1} (**TS-2H$_{(f\rightarrow c)}$**$^+$). When **2H$_c$**$^+$ is formed (20 kJ mol^{-1}), $NO_2^{\bullet}$ loss can occur through homolysis of the σ-bond between the two nitrogens, N(2)–N(4), with the formation of the final radical **2H$_j$**$^{+\bullet}$ (89 kJ mol^{-1}). Alternatively, loss of neutral HNO_2 can be achieved through a third process involving two-steps. The first step involves isomerization of **2H$_c$**$^+$ to **2H$_h$**$^+$. In principle this might involve two discreet transition states: (i) a 1,5-intramolecular proton transfer of the N(1) proton to the oxygen O(1); (ii) axial rotation on the bond N(4)–O(1). However, only a single transition state **TS-2H$_{(c\rightarrow h)}$**$^+$ at 168 kJ mol^{-1} could be found, and IRC calculations connected this transition state to both **2H$_c$**$^+$ to **2H$_h$**$^+$. This either suggests a concerted process to isomerize **2H$_c$**$^+$ to **2H$_h$**$^+$, or that intramolecular proton transfer of the N(1) proton to the oxygen O(1) is barrierless. The second step involves heterolytic cleavage of the N(2)–N(4) bond in **2H$_h$**$^+$ *via* transition state **TS-2H$_{(h\rightarrow i)}$**$^+$ at 204 kJ mol^{-1} to generate the product ion **2H$_i$**$^+$, with an overall endothermicity of 112 kJ mol^{-1}. The loss of neutral HNO_2 and the radical $NO_2^{\bullet}$ can occur from either **2H$_f$**$^+$ or **2H$_a$**$^+$, but formation of the final products **2H$_l$**$^+$ and **2H$_k$**$^{+\bullet}$ is very endothermic (250 and 200 kJ mol^{-1} respectively).

The alternative mechanism for HNO_2 loss (Fig. S5†) follows the same intramolecular H-transfer from N(1) to O(1) described for the water loss mechanism given in Fig. S5,† but it involves a different transition state with an activation barrier of 253 kJ mol^{-1}, and is thus is also unlikely to happen. Even if the final products **2H$_i$**$^+$ and **2H$_j$**$^{+\bullet}$ are located at lower energetic levels compared to **4**$^+$, the losses of neutral HNO_2 and the radical $NO_2^{\bullet}$ cannot readily occur under low energy CID conditions due to the higher barriers required.

Discussion

How the increased contribution of resonance form A2 influences both the crystal structure of 2 relative to 1 as well as the gas phase chemistry of 2H$^+$ compared to 1H$^+$

X-ray crystal structure of 2 relative to 1. The synthesis of the metabolite olefin–imidacloprid **2** allowed a comprehensive analysis of its properties *via* X-ray crystallography and mass spectrometry. The crystallographic analysis of **2** highlighted how the installation of an imidazole ring system adjacent to the nitroguanidinyl moiety can perturb the balance between the two resonance forms, which also drastically changes the preferred fragmentation reaction of **2H**$^+$ in the gas phase. A search of the Cambridge Crystallographic Database for molecules containing a nitroguanidine moiety gave 151 hits, of which 132 existed in the tautomeric form **A** (Scheme 2), which is also adopted by both imidacloprid **1** and olefin–imidacloprid **2**.[23] Within this tautomer there is extensive delocalisation of the amino nitrogen lone pairs onto the oxygen atoms of the nitro group through the imine which can be represented by the two resonance forms **A1** and **A2**. A comparison of the N–N and C–N bond distances on the 'nitro tail' of both compounds suggested a significantly greater contribution of form **A2** in compound **2** while compound **1** shows a greater contribution from resonance form **A1**.[24]

Sites of protonation in 1 and 2. Given the greater contribution of resonance form **A2** in **2** compared to **1**, we wondered if this might influence the proton affinities (PA) on the different heteroatoms (N and O) already studied in imidacloprid and the gas-phase fragmentation reactions of **1H**$^+$.[22] The local PAs of **2** were calculated using Gaussian09 with the B3YLP level of theory and the 6-311G++(d,p) basis set to permit a comparison with **1**. Although the N(5) remains the thermodynamically favoured site of ionisation, the relative PAs for the N and O heteroatoms in **2** are generally lower than for **1** (Table 1). The greatest difference resides in O(2) where olefin–imidacloprid shows a relative PA of 9 kJ mol^{-1} compared to the 32 kJ mol^{-1} of **1H**$^+$. This result indicates that the oxygen atom of the nitro group not involved in the hydrogen bond with N(1)–H binds a proton more tightly in **2H**$^+$. The N(2) site does not show a great difference between compound **1H**$^+$ and **2H**$^+$ with relative PAs of 24 and 20 kJ mol^{-1} respectively. The

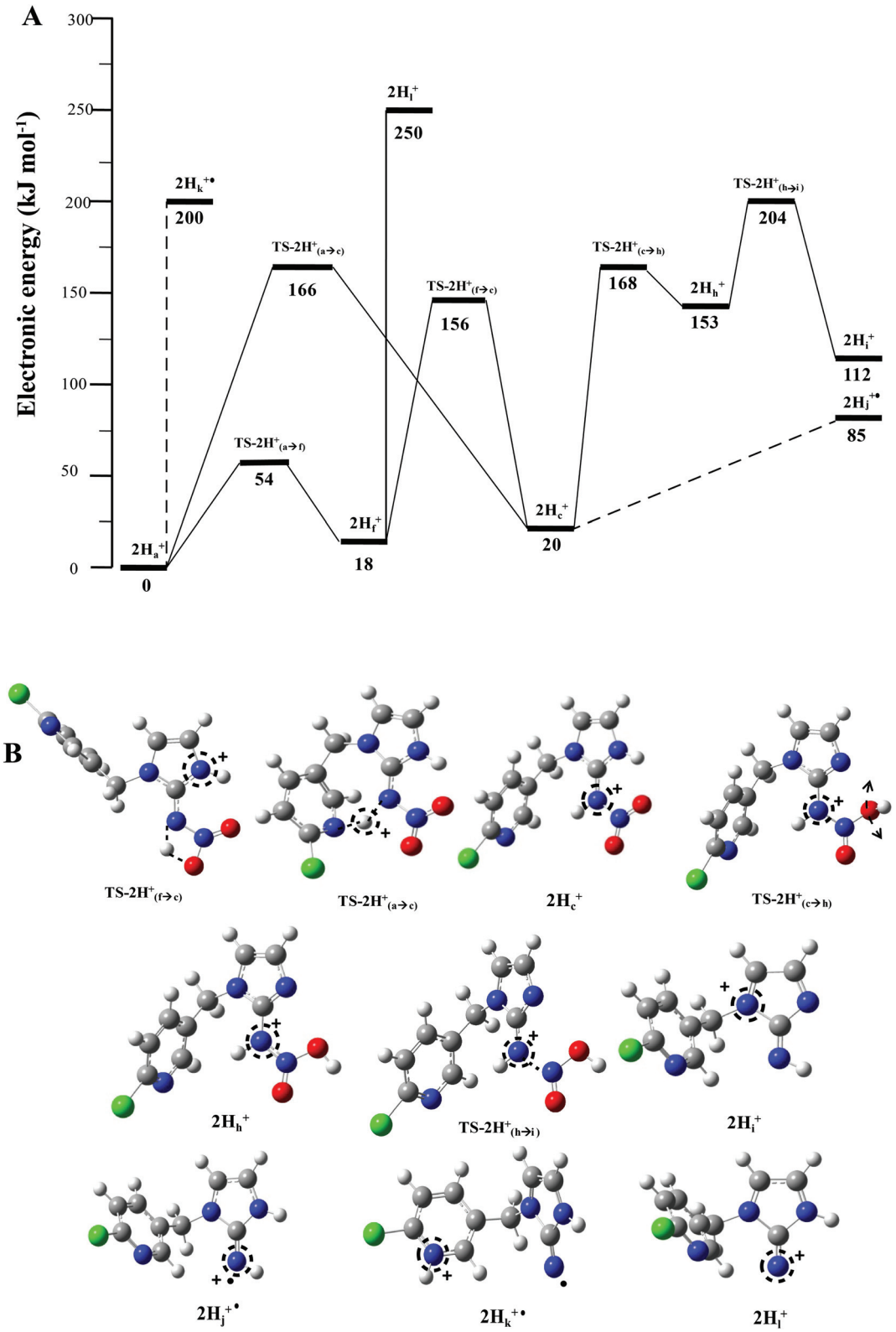

Fig. 5 B3LYP/6-311G++(d,p) DFT calculated mechanisms for competing $NO_2^{\bullet}$ and HNO_2 losses from $2H^+$: (A) potential energy diagram. (B) Structures of key species. Energetic levels connected by dash lines indicate bond homolysis reactions where it was not possible to optimize a transition state.

Table 1 Key DFT calculated thermochemical differences (in kJ mol^{-1}) relevant to the gas-phase fragmentation of $1H^+$ and $2H^+$

	$1H^+$	$2H^+$
Proton affinities		
Relative PA for N(5) site	0	0
Relative PA for N(2) site	24	20
Relative PA for O(1) site	Not calculated	27
Relative PA for O(2) site	32	9
Relative PA for N(3) site	109.8	Not calculated
Relative PA for N(1) site	122	193
ΔE $NO_2^{\bullet}$ *loss*		
Protonation site on N(5)	182	200
Protonation site on N(2)	150	89
Energy activation barriers		
Proton transfer from N(5) to O(2)	68	54
Proton transfer from N(5) to N(2)	175	166
Proton transfer from O(2) to N(2)	163	156
Rotation N–N bond O(2)–H	Not calculated	117
Proton transfer from N(5) to O(1)	Not calculated	119
Proton transfer from O(2) to O(1)	Not calculated	145

higher PA for the O(2) position of **2** is consistent with the predominance of resonance form **A2**, which makes the oxygen on the nitro group more basic whilst maintaining the same sp^2 hybridization state for N(2). The installation of an imidazole ring in **2** significantly reduces the relative PA in N(1) (193 *versus* 122 kJ mol^{-1}) and protonation of nitrogen N(3) results in cleavage of the N(3)–C(4) bond.

Gas phase chemistry of $2H^+$ compared to $1H^+$. The main gas-phase fragmentation reaction of $2H^+$ under low-energy CID involves loss of H_2O (*m*/*z* 236), with competing losses of $NO_2^{\bullet}$ (*m*/*z* 208) and HNO_2 (*m*/*z* 207) being less important. Loss of water is unique to $2H^+$, with $1H^+$ fragmenting instead *via* losses of $NO_2^{\bullet}$, N_2O and $NO^{\bullet}$.[22] The fragmentation mechanism of nitroguanidine and its derivatives have been reported in the literature showing that these moieties lose predominantly $NO_2^{\bullet}$ followed by H_2O.[36] A recent study on low energy CID of protonated 2-nitroimidazole showed that the major loss of water occurs: (i) from the position of the NO_2 substituent on the imidazole; and (ii) *via* a series of 1,4-intramolecular proton transfer coupled by a 180° rotation of the NO_2 functional group.[33] The two hydrogen atoms involved in water loss from $2H^+$ are the ionizing proton located on N(5) and the N(1)–H, as confirmed by a H/D exchange reaction on compound **2**. Thus, when the deuterated form $[M - H + 2D]^+$ at *m*/*z* 256 was mass selected and fragmented with the same CID conditions applied for $2H^+$, the product ion at *m*/*z* 236 was regenerated demonstrating that $[M - H + 2D]^+$ underwent loss of D_2O in the gas-phase.

DFT calculations of $2H^+$ compared to $1H^+$. DFT calculations were used to examine possible mechanisms associated with the loss of water (Fig. 4). Three main mechanisms were found, two of which involved a rotation of the N(2)–N(4) bond related to that which has been described for protonated 2-nitroimidazole.[33] From the ground state $2H_a^+$ the ionizing proton on the pyridine N atom is first transferred to the O(2) of the nitro group to give $2H_b^+$, a reaction previously described for $1H^+$.[22] $2H_b^+$ then undergoes a rotation about the N(2)–N(4) bond *via* **TS-2H$_{(b\rightarrow d)}^+$** at 117 kJ mol^{-1} to give $2H_d^+$, which then undergoes dissociative 1,5-intramolecular proton transfer *via* **TS-2H$_{(d\rightarrow g)}^+$** to trigger the release of water, generating 4^+, with an overall reaction endothermicity of 123 kJ mol^{-1}.

The other two possible competing mechanisms for loss of water involve alternative direct transfer of the ionizing proton from N(5) to O(2) *via* the transitions state **TS-2H$_{(a\rightarrow d)}^+$** with a barrier of 119 kJ mol^{-1} and the 1,3-intramolecular proton transfer *via* the **TS2-2H$_{(b\rightarrow d)}^+$** with a barrier of 145 kJ mol^{-1}. Since all these three mechanisms possess barriers lower than those described for the competing losses of $NO_2^{\bullet}$ and HNO_2 (Table 1), they are likely to operate simultaneously, which offers a reason why 4^+ increases with the increase of the energy in the energy-resolved CID experiments (Fig. 2B), while the relative intensities of the product ions $2H_i^+$ and $2H_j^{+\bullet}$ are maintained.

For $1H^+$, the losses of $NO_2^{\bullet}$ and HNO_2 also only occur when the proton is transferred to the nitrogen N(2). The transfer of the proton from N(5) to N(2) (*via* **TS-2H$_{(a\rightarrow c)}^+$** at 166 kJ mol^{-1}) or from O(2) to N(2) (*via* **TS-2H$_{(f\rightarrow c)}^+$** at 156 kJ mol^{-1}) in $2H^+$ require significantly higher energies compared to all three mechanisms involved in water loss. Furthermore, the contributing resonance form **A2** that characterizes compound **2** means that more energy is required to break the N(2)–N(4) bond to allow the final release of HNO_2 (*via* **TS-2H$_{(h\rightarrow i)}^+$** at 204 kJ mol^{-1}). $NO_2^{\bullet}$ and HNO_2 loss can occur directly from $2H_a^+$ and $2H_f^+$ but as for $1H^+$, the final products are energetically unfavourable. The CID spectrum of $1H^+$ also shows losses of N_2O and $NO^{\bullet}$ from the nitroguanidine group.

The challenge of assigning structures of small molecule natural products and metabolites from comparisons of CID spectra of related species

Since the late 1950s, mass spectrometry has played a key role in determining the structures of small organic molecules.[37,38] It was rapidly recognized that the fragment ions formed under conditions of electron ionization (EI) provided a unique "structural fingerprint", which led to the development of EI/MS libraries (databases)[39,40] and the use of computer assisted structure elucidation, as pioneered by the late Carl Djerassi.[41] The use of automated tools for the identification of small molecules from MS data is emerging as a key way of dealing with: (i) the vast amounts of data in metabolomics; and (ii) dereplication of "hits" in the field of natural products chemistry. Since spectral libraries only contain known reference compounds, they will always be incomplete. Thus, there is a push to seek alternative methods to replace searching in spectral libraries by searching molecular structure databases such as PubChem and KEGG (Kyoto Encyclopedia of Genes and Genomes) and using these to create *in silico* spectral libraries based on programs that use empirical "rules" to predict gas-phase fragmentation behavior.[42] Often these programs predict fragmentation based on the similarities of substructures, but the differences in fragmentation behavior

of $1H^+$ and $2H^+$ clearly highlight the challenges of such an empirical approach. Thus there is a continued need to adopt a "physical organic" approach to understand how structure dictates which fragmentation pathways are the lowest in energy.[43] With ever increasing computer speeds, it may be possible to predict tandem mass spectra using computational chemistry approaches similar to those being developed by Grimme for EI mass spectra.[44]

Experimental methods

Chemicals

All chemicals were used as purchased. Acetonitrile, ethyl acetate and hexane were obtained from Merck (Kenilworth, NJ, USA). Acetic acid (glacial) was obtained from BDH (Poole, Great Britain). Deuterated water (D_2O), acetonitrile-d_3 and acetic acid-d_4 were purchased from Cambridge Isotopes Laboratories (Andover, MA, USA). 2,2-Diethoxyethanamine and 2-chloro-5-chloromethylpyridine were obtained from Sigma-Aldrich (Saint Louis, United States). *S*-Methyilisothiouronium sulphate salt was purchased from Alfa Aesar (Heysham, Great Britain). Analytic grade ether was purchased from Chemsupply (Port Adelaide, SA, Australia).

Synthesis of 2

The synthesis of olefin–imidacloprid **2** (ESI, Scheme S1†) was reproduced using the same method described by Novák *et al.*[14,21] Full details of the synthesis and the characterization of key intermediates are given in the ESI.†

X-ray crystallography of 2

The crystal structure of the final product **2** was determined on an Oxford SuperNova CCD diffractometer using Cu-Kα radiation (graphite crystal monochromators λ = 1.54184 Å). The crystal was maintained at 130.0 K during data acquisition. The structure was solved by direct methods and difference Fourier Synthesis[45] Thermal ellipsoid plots were generated using the program ORTEP-3 [46] integrated within the WINGX suite of programs.[47] Crystal data for **2** $C_9H_8N_5O_2Cl$, M 253.65, T = 130.0(2) K, λ = 1.5418 Å, monoclinic, space group $P21/c$, a = 4.7377(5), b = 21.5338(19), c = 10.5144(8)Å, β = 101.413(9)°, V = 1051.48(17) Å^3, Z = 4, D_c = 1.602 Mg M^{-3} μ(Cu-Kα) = 3.244 mm^{-1}, $F(000)$ = 520, crystal size 0.51 × 0.05 × 0.05 mm. θ_{max} = 74.29°, 4222 reflections measured, 2081 independent reflections (R_{int} = 0.050) the final R = 0.0525 [$I > 2\sigma(I)$, 1659 data] and w$R(F^2)$ = 0.1554 (all data) GOOF = 1.091.

Mass spectrometry experiments

Linear ion trap. Mass spectrometry experiments were carried out using a hybrid linear ion trap and 7 T Fourier transform ion cyclotron resonance (FT-ICR) mass spectrometer (Finnigan LTQ-FT, Bremen, Germany), equipped with an electrospray ionization source. A 0.4 mM solution of **2** in a 70 : 30 : 0.1% acetonitrile : water : formic acid mixture was introduced into the electrospray source at a flow-rate of ~3 μL min^{-1} using a syringe pump. Typical electrospray conditions were employed using a needle potential of ~+4 kV and a heated capillary temperature of 300 °C. The $2H^+$ was mass selected with a window of 1 m/z and then subjected to CID using a corresponding normalized collision energy of 20% and an activation Q of 0.25 for a period of 30 ms. For high accuracy mass measurements, the fragment ions are formed and isolated in the linear ion trap, and transferred to the FT-ICR MS for measurement of the m/z values with a mass accuracy that is sub part-per-million, providing unambiguous assignment of the stoichiometry of the precursor and fragment ions.

Energy resolved CID experiments in the 3D ion trap. The energy resolved CID studies on compound **2** were carried out in a Finnigam 3D ion trap (LCQ) mass spectrometer (Finnigan Mat, Bremen, Germany) as described by Colorado and Brodbelt.[48] A 0.4 mM solution of compound **2** in a 70 : 30 : 0.1% acetonitrile : water : formic acid mixture was introduced into the electrospray source at a flow-rate of ~3 μL min^{-1} *via* a syringe pump system. The conditions used to ionize the compound were set as follow: spray voltage +3.5–4.0 kV, capillary temperature 250 °C, capillary voltage 25 V, nitrogen sheath gas pressure 50 (arbitrary unites). A selection window of 1 m/z and an activation Q of 0.25 for a period of 30 ms were used. $2H^+$ was mass selected in the gas phase and the normalised collision energy (NCE) was increased stepwise by 1.0% starting from 0% (no product ion formed) to a maximum of 30% (the relative intensity of the precursor ion was less than 5%). The NCE was converted to an amplitude of the resonance excitation RF voltage (tick amp) using the follow equation:

$$\text{Amplitude (V)} = \frac{(\text{NCE\%})}{30\% \times [(\text{Parent mass}) \times (\text{Tickamp slope}) + \text{tick amp intercept}]}$$

The tick amp slope and tick amp intercept are extracted from the normalised collision energy calibration file of the most recent calibration. The relative intensity of the product and precursor ions was plotted as a function of the increasing amplitude expressed in voltage.

CID experiments in QTof mass spectrometer. CID experiments on compound **2** were carried out using an Agilent 6520 Q-TOF mass spectrometer (Agilent Technologies, Inc., Santa Clara, CA, USA). 10 μL of a 0.02 mM solution of compound **2** dissolved in 100% ACN, was mixed with a 70 : 30 : 0.1% acetonitrile : water : formic acid mixture into a 100 μL HPLC injection loop using the Agilent 1100 autosampler. Sample was introduced in the mass spectrometer at the flow-rate of 0.3 mL min^{-1}. Ionisation of $2H^+$ was obtained using a dual-nebulizer ESI source with the capillary voltage set at +3 kV, gas temperature (nitrogen) set at 300° C, dry gas at 12 L min^{-1} and nebulizer at 50 psig. The fragmentor and the skimmer were set at 120 and 65 V respectively to induce the ionisation of $2H^+$ avoiding ion source fragmentation.

$2H^+$ was mass selected in the quadrupole using a selection window of 1.3 *m/z* to exclude the ^{37}Cl-isotope pick at *m/z* 256. CID was performed applying increasing CID energy from 5 to 20% till $2H^+$ was less than 5% of its original intensity in the MS/MS spectrum.

Hydrogen/deuterium exchange of 2. The H/D exchange reaction was performed by suspending compound **2** in a 70 : 29 : 1 D_2O : acetonitrile-d_3 : acetic acid-d_4 mixture for 2 h at room temperature. The addition of acetic acid-d_4 to the mixture helped the exchange of the N(1)–H with deuterium. Using the hybrid linear ion trap with the same settings described above, $[M - H + 2D]^+$ was mass selected (*m/z* 256) and fragmented under identical CID conditions used for $2H^+$. Even though the H/D exchange was not complete in solution as evidenced by the presence of $2H^+$ in the mass spectrum, the HRMS information obtained from the FT-ICR helped to distinguish among the compounds derived from the fragmentation of $[M - H + 2D]^+$ and the fragmentation of the ^{37}Cl isotope of $2H^+$ (*m/z* 256.05648 and 256.04098 respectively) which cannot be distinguished and isolated in the ion trap.

DFT calculations

The coordinates from the crystal structure of **2** were used as a starting point for our computational analysis. We carried out molecular dynamic (MD) simulations using the Discovery Studio (DS) 2.5 program package and the method settings described in a previous work[34] to provide stable structures for compound **2** in the gas-phase. At completed simulation, the 10 most stable structures were selected and further optimized in Gaussian 09 to refine the previous result and find the lowest energy structure. Rotations of 90° of the 'nitroimine chain' of the guanidine moiety were used to establish which tautomeric form was more stable and the role played by the hydrogen bond N(1)–H···O(1) in the stability of compound **2** in the gas-phase. A 360° scan on the dihedral angle D1 (Scheme 1) was carried out to confirm the position of the nitrogen N(5) on the pyridine in relation to the nitroguanidine moiety. The final optimised structure was used to determine the local PAs for the different heteroatom (N and O) and the barriers involved in the gas-phase fragmentation reactions of $2H^+$. DFT calculations were carried out using Gaussian 09 with the B3LYP level of theory and the 6-311G++(d,p) basis set to allow a direct comparison with compound $1H^+$.[22] The vibrational frequencies of each DFT optimized structure were calculated to ensure they were either minima (all positive) or transition state structures (one negative frequency). Transition states were connected to reactants and products *via* intrinsic reaction coordinate (IRC) calculations. The Electronic energies reported are relative to the ground state structure of $2H^+$ (0 kJ mol^{-1}). The transition state associated with bond homolysis ($NO_2^{\bullet}$ loss) was not calculated due to the challenges on moving from a singlet electronic ground state to doublet products. Thus dashed lines are used to connect $2H^+$ to the final energies of the radical products.

Conclusions

The structure/reactivity of olefin–imidacloprid **2** compared to the parent insecticide imidacloprid **1**, was revealed using X-ray crystallography, tandem mass spectrometry and DFT calculations. A comparison of the X-ray structure of compounds **1** and **2** with 132 similar nitroguanidine containing compounds deposited in the Cambridge database, highlights that both compounds prefer tautomeric forms **A**. However, an analysis of the bond lengths at the nitroguanidine residue showed that the shorter N(3)–N(4) bond and the longer C(1)–N(2) bond of **2** best fit resonance form **A2** while imidacloprid more closely resembles resonance form **A1**. These differences underpin the distinct gas-phase fragmentation reactions of $1H^+$ and $2H^+$. Thus the contribution of resonance form **A2** makes (i) the oxygen atom O(2) more basic and (ii) the nitrogen N(1) more acidic. The increased basicity in O(2) is the reason why the 1,3-intramolecular proton transfer to N(2) or between the two oxygen atoms requires higher energies of 156 and 145 kJ mol^{-1} respectively compared to 117 kJ mol^{-1} required to rotate the NO_2 group by 180°. With the oxygen positioned next to N(1)–H, a 1,5-intramolecular proton transfer can occur. As the $NO_2^{\bullet}$ and HNO_2 losses can only occur in $2H^+$ when the proton has been transferred on N(2), their relative abundance is minor (no more that 30% of total product ions). The use of multi-stage low-energy CID conditions established that: (i) water loss is the main fragmentation channel of $2H^+$; (ii) the product ions at *m/z* 205 and 171 used in MRM studies are likely to arise from sequential fragmentation reactions.

Acknowledgements

We thank the Australian Research Council for financial support *via* the ARC Centre of Excellence for Free Radical Chemistry and Biotechnology (CE0561607). Roberto Fusetto thanks The University of Melbourne for a postgraduate scholarship and Michael Leeming and Athanasios Zavras for their support with the DFT calculations. We thank Dr W. Alex Donald and Huixin Wang from the University of New South Wales for their help with the molecular dynamic simulations. For generously providing computational resources high-performance computing facilities, we thank the Victorian Partnership for Advanced Computing and the School of Chemistry at the University of Melbourne.

References

1 P. Jeschke, R. Nauen, M. Schindler and A. Elbert, *J. Agric. Food Chem.*, 2011, **59**, 2897–2908.
2 M. Tomizawa and J. E. Casida, *Acc. Chem. Res.*, 2009, **42**, 260–269.
3 M. Tomizawa and J. E. Casida, *J. Agric. Food Chem.*, 2011, **59**, 2825–2828.

4 D. Carrington, *Pesticides Linked to Honeybee Decline*, in The Guardian, 2012.
5 P. R. Whitehorn, S. O'Connor, F. L. Wackers and D. Goulson, *Science*, 2012, **336**, 351–352.
6 M. Gross, *Curr. Biol.*, 2013, **23**, R462–R464.
7 I. Yamamoto, *Nicotinoid Insecticides and the Nicotinic Acetylcholine Receptor*, Springer, Tokyo, 1999.
8 J. E. Casida, *J. Agric. Food Chem.*, 2011, **59**, 2923–2931.
9 M. A. Riaz, A. Chandor-Proust, C. Dauphin-Villemant, R. Poupardin, C. M. Jones, C. Strode, M. Régent-Kloeckner, J. P. David and S. Reynaud, *Aquat. Toxicol.*, 2013, **126**, 326–337.
10 S. Suchail, L. Debrauwer and L. P. Belzunces, *Pest Manage. Sci.*, 2004, **60**, 291–296.
11 M. Tomalski, W. Leimkuehler, C. Schal and E. L. Vargo, *Ann. Entomol. Soc. Am.*, 2010, **103**, 84–95.
12 H. Nishiwakl, K. Sato, Y. Nakagawa, M. Miyashlta and H. Miyagawa, *J. Pesticide Sci.*, 2004, **29**, 110–116.
13 K. K. Hoi, P. J. Daborn, P. Battlay, C. Robin, P. Batterham, R. A. J. O'Hair and W. A. Donald, *Anal. Chem.*, 2014, **86**, 3525–3532.
14 T. T. Talley, M. Harel, R. E. Hibbs, Z. Radić, M. Tomizawa, J. E. Casida and P. Taylor, *Proc. Natl. Acad. Sci. U. S. A.*, 2008, **105**, 7606–7611.
15 S. L. Chao and J. E. Casida, *Pestic. Biochem. Physiol.*, 1997, **58**, 77–88.
16 A. Rocher and N. Marchand-Geneste, *SAR QSAR Environ. Res.*, 2008, **19**, 245–261.
17 M. Ihara, T. Okajima, A. Yamashita, T. Oda, K. Hirata, H. Nishiwaki, T. Morimoto, M. Akamatsu, Y. Ashikawa, S. Kuroda, R. Mega, S. Kuramitsu, D. B. Sattelle and K. Matsuda, *Invertebr. Neurosci.*, 2008, **8**, 71–81.
18 H. Nishiwaki, Y. Nakagawa, M. Kuwamura, K. Sato, M. Akamatsu, K. Matsuda, K. Komai and H. Miyagawa, *Pest Manage. Sci.*, 2003, **59**, 1023–1030.
19 S. Kagabu, C. Kato and K. Nishimura, *J. Pesticide Sci.*, 2004, **29**, 376–379.
20 Y. J. Dai, S. Yuan, F. Ge, T. Chen, S. C. Xu and J. P. Ni, *Appl. Microbiol. Biotechnol.*, 2006, **71**, 927–934.
21 L. Novák, G. Hornyánszky, I. Király, J. Rohály, P. Kolonits and C. Szántay, *Heterocycles*, 2001, **55**, 45–58.
22 W. A. Donald, M. G. Leeming and R. A. J. O'Hair, *Int. J. Mass Spectrom.*, 2012, **316**, 91–99.
23 F. H. Allen, *Acta Crystallogr., Sect B: Struct. Sci.*, 2002, **58**, 380–388.
24 D. Chopra, T. P. Mohan, K. S. Rao and T. N. G. Row, *Acta Crystallogr., Sect. E: Struct. Rep. Online*, 2004, **60**, o2415–o2417.
25 Y. Qin, P. Zhao, S. Fan, Y. Han, Y. Li, N. Zou, S. Song, Y. Zhang, F. Li, X. Li and C. Pan, *J. Chromatogr., A*, 2015, **1385**, 1–11.
26 S. Fan, P. Zhao, C. Yu, C. Pan and X. Li, *Food Addit. Contam., Part A Chemistry, Analysis, Control, Exposure and Risk Assessment*, 2014, **31**, 73–82.
27 S. H. Tseng, C. C. Liu, Y. J. Lin, H. C. Chen, S. C. Su, H. K. Chou, S. S. Chou and D. Y. C. Shih, *J. Food Drug Anal.*, 2009, **17**, 319–332.
28 C. Jabot, M. Fieu, B. Giroud, A. Buleté, H. Casabianca and E. Vulliet, *Int. J. Environ. Anal. Chem.*, 2015, **95**, 240–257.
29 M. Gbylik-Sikorska, T. Sniegocki and A. Posyniak, *J. Chromatogr., B: Anal. Technol. Biomed. Life Sci.*, 2015, **990**, 132–140.
30 M. Eckert-Maksić, Z. Glasovac, H. Maskill and I. Zrinski, *J. Phys. Org. Chem.*, 2003, **16**, 491–497.
31 L. G. Cabrini, M. Benassi, M. N. Eberlin, T. Okazaki and K. K. Laali, *Eur. J. Org. Chem.*, 2007, 70–77.
32 A. Giordana, G. Ghigo, G. Tonachini, D. Ascenzi, P. Tosi and G. Guella, *J. Chem. Phys.*, 2009, 131.
33 L. Feketeova, J. Postler, A. Zavras, P. Scheier, S. Denifl and R. A. J. O'Hair, *Phys. Chem. Chem. Phys.*, 2015, **17**, 12598–12607.
34 H. Wang, B. Wang, Z. Wei, H. Zhang and X. Guo, *J. Mass Spectrom.*, 2015, **50**, 212–219.
35 R. A. J. O'Hair, P. S. Broughton, M. L. Styles, B. T. Frink and C. M. Hadad, *J. Am. Soc. Mass Spectrom.*, 2000, **11**, 687–696.
36 V. Borrett, I. Dagley, M. Kony and T. Blumenthal, *Eur. J. Mass Spectrom.*, 1995, **1**, 59–64.
37 J. H. Beynon, *Org. Mass Spectrom.*, 1968, **1**, 739–740.
38 K. Biemann, *Mass spectrometry: organic chemical applications*, McGraw-Hill, 1962.
39 Wiley Specialty Mass Spectral Libraries, http://www.sisweb.com/software/ms/wiley.htm.
40 NIST 14 Mass Spectral Library, http://www.sisweb.com/software/ms/nist.htm.
41 B. G. Buchanan, D. H. Smith, W. C. White, R. J. Gritter, E. A. Feigenbaum, J. Lederberg and C. Djerassi, *J. Am. Chem. Soc.*, 1976, **98**, 6168–6178.
42 F. Hufsky, K. Scheubert and S. Böcker, *Nat. Prod. Rep.*, 2014, **31**, 807–817.
43 G. Bouchoux, *J. Mass Spectrom.*, 2013, **48**, 505–518.
44 S. Grimme, *Angew. Chem., Int. Ed.*, 2013, **52**, 6306–6312.
45 G. Sheldrick, *Acta Crystallogr., Sect. A: Fundam. Crystallogr.*, 2008, **64**, 112–122.
46 L. Farrugia, *J. Appl. Crystallogr.*, 1997, **30**, 565.
47 L. Farrugia, *J. Appl. Crystallogr.*, 1999, **32**, 837–838.
48 A. Colorado and J. Brodbelt, *J. Am. Soc. Mass Spectrom.*, 1996, **7**, 1116–1125.